Journal of Oceanography, Vol. 63, pp. 863 to 872, 2007

Short Contribution

Effect of Air-Sea Temperature Difference on Ocean Microwave Brightness Temperature Estimated from AMSR, SeaWinds, and Buoys

AKIRA SHIBATA*

Earth Observation Research Center, Japan Aerospace Exploration Agency, Sengen, Tsukuba 305-8505, Japan

(Received 10 July 2006; in revised form 13 February 2007; accepted 14 April 2007)

The effect of air-sea temperature differences on the ocean microwave brightness temperature (Tb) was investigated using the Advanced Microwave Scanning Radiometer (AMSR) aboard the Advanced Earth Observing Satellite-II (ADEOS-II) during a period of seven months. AMSR Tb in the global ocean was combined with wind data supplied by the scatterometer SeaWinds aboard ADEOS-II and air temperature given by a weather forecast model. Tb was negatively correlated with air-sea temperature difference, its ratio lying around –0.4K/°C at the SeaWinds wind speed of 14 m/s for the 6 GHz vertical polarization. Tb of AMSR-E aboard AQUA during 3.5 years was combined with ocean buoy data, and similar results were obtained.

Keywords:
· AMSR,
· ADEOS-II,
· AQUA,
· air-sea temperature difference,
· ocean microwave brightness temperature.

1. Introduction

In our previous paper (Shibata, 2006), we described a method of correcting the wind effect on the ocean microwave brightness temperature (Tb), which is used in an algorithm to retrieve the sea surface temperature (SST) from the Advanced Microwave Scanning Radiometer (AMSR). We pointed out in that paper that a wind correction coefficient used in the SST algorithm varies both seasonally and latitudinally in the global ocean. In addition, we identified two regions where different coefficients should be applied: the Arabian Sea in summer, where the air-sea temperature difference is positive; and the northern western Atlantic Ocean in winter, where the air-sea temperature difference is negative. Furthermore, we noticed that monthly averaged Tb (defined in Section 3) vary from month to month between the northern and southern hemispheres, and also between the ascending- and descending-orbit data, while their behavior was not sufficient well understood for publication. We then inferred that these Tb variations might be caused by the air-sea temperature difference. The purpose of the present paper is therefore to obtain a relation between the ocean Tb and air-sea temperature difference in the global ocean, and then to improve the AMSR SST using this relation.

The ocean Tb under calm conditions is expressed by the Fresnel formula. It is a function of frequency, polarization, incidence angle, SST, and salinity (Swift, 1980). For a rough ocean surface, both experimental and theoretical studies have been performed (Hollinger, 1971; Wentz, 1983; Meissner and Wentz, 2002). The air-sea temperature difference has not been considered as an additional parameter describing the ocean Tb. Before start to describe our research, we should draw attention to two previous works: one by Droppleman (1970) reporting that the ocean Tb rises significantly when ocean foam is present, because the emissivity of the ocean foam is much higher than that of the ocean surface, and the other by Monaham and O'muircheartaigh (1986), reporting that the whitecap coverage of the ocean surface varies with wind speed, SST, and air-sea temperature difference. In our discussion of this paper we relate our results to these earlier reports.

This work is mainly based on data from two sensors: AMSR and a NASA scatterometer SeaWinds, both aboard the Advanced Earth Observing Satellite-II (ADEOS-II) launched by the Japan Aerospace Exploration Agency (JAXA) in December 2002. SeaWinds observes the Earth's surface to retrieve the ocean wind vector (Liu, 2002). The SeaWinds ocean wind vector is helpful in analyzing the AMSR Tb related to ocean wind, and to air-sea temperature differences.

* E-mail address: shibata.akira@jaxa.jp

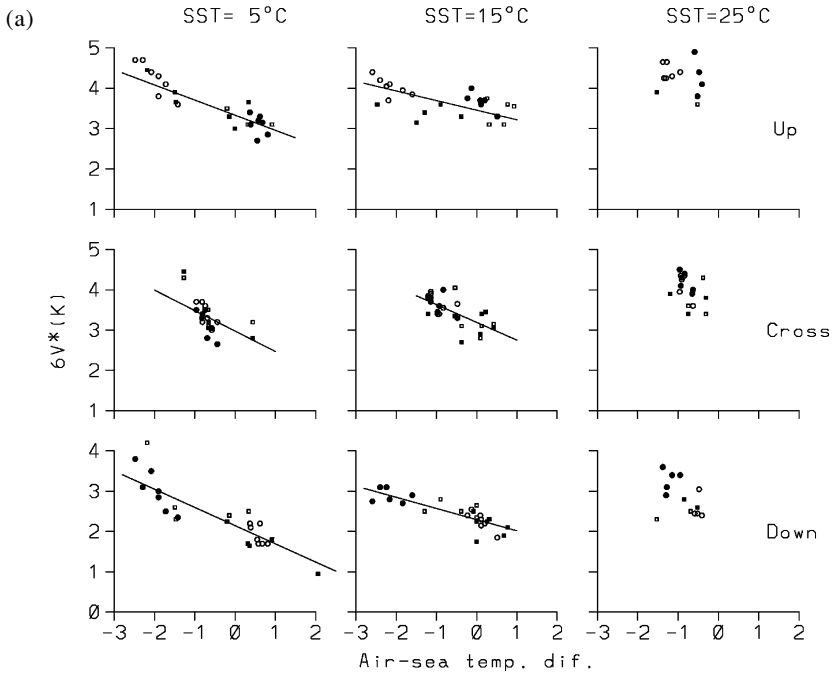

Fig. 1. (a) Relations between 6V* and air-sea temperature difference at three SSTs in three relative wind directions, obtained at SeaWinds wind speed of 14 m/s, (b) the same values for 6H*.

2. Sensors and Data

AMSR is a forward-looking, conically scanning radiometer positioned at a constant-incidence angle of 55° (Kawanishi *et al.*, 2003). The AMSR frequencies are 6, 10, 18, 23, 36, 50, 52, and 89 GHz. There are two polarizations (V-pol and H-pol) at all frequencies, except for 50 and 52 GHz, at which only V-pol is available. The diameter of AMSR's main antenna is 2 m, and it rotates at 40 rpm. The spatial resolution on the Earth's surface at 6 GHz is 40×70 km, and 3×6 km at 89 GHz. The spatial sampling interval on the Earth's surface is 10 km at all frequencies except for 89 GHz, at which it is 5 km. In one rotation (360°) of the antenna, the AMSR observes the Earth during scanning angles between –61° and 61°, where 0° means the forward direction of the ADEOS-II flight.

The SeaWinds emits microwave signals and measures backscattered signals from the Earth's surface. The signal from the ocean surface is related to capillary waves or short gravity waves with a wavelength of several centimeters on the ocean surface. The ocean wind vector (speed and direction) can be retrieved by the scatterometer model function relating the signal to buoy wind data (Liu, 2002). The anemometer heights of buoys are different as between buoy types. The buoy wind speeds are usually corrected to 10 meter height wind speeds assuming neutral atmospheric conditions (Liu and Tang, 1996). The SeaWinds wind data were validated according to this equivalent neutral wind of buoys at 10 m height (Ebuchi, 2006). We used the Level 2B geophysical data of SeaWinds with a spatial resolution of 25 km. Unfortunately, ADEOS-II stopped operating in October 2003 due to a failure of an electronic cable from a solar panel. Data were therefore available for seven months from April to October 2003.

We need to know the SST and air temperature on the ocean surface in order to determine the air-sea temperature difference. We used the Reynolds SST of weekly analysis (Reynolds and Smith, 1994). The spatial resolution of the Reynolds SST is 2°, and it was interpolated spatially into 0.25° interval grids, and temporally into one day intervals. The air temperature was adopted from the weather-forecast model of the Japan Meteorological Agency (JMA), known as the Global Analysis (GANAL). The spatial resolution of the GANAL is 1.25° in both longitude and latitude directions. The GANAL time interval is six hours, resulting in four data points per day. We interpolated these spatially into 0.25° interval grids. The air temperature measurement height is 2 m above the ocean surface.

We also use the air temperature measured by ocean buoys, since the accuracy of the GANAL air temperature might not be adequate for our studies. Buoy data were collected from the National Data Buoy Center (NDBC), Tropical Atmosphere Ocean (TAO), and PIRATA. Selected buoys were confined to the open ocean off 100 km

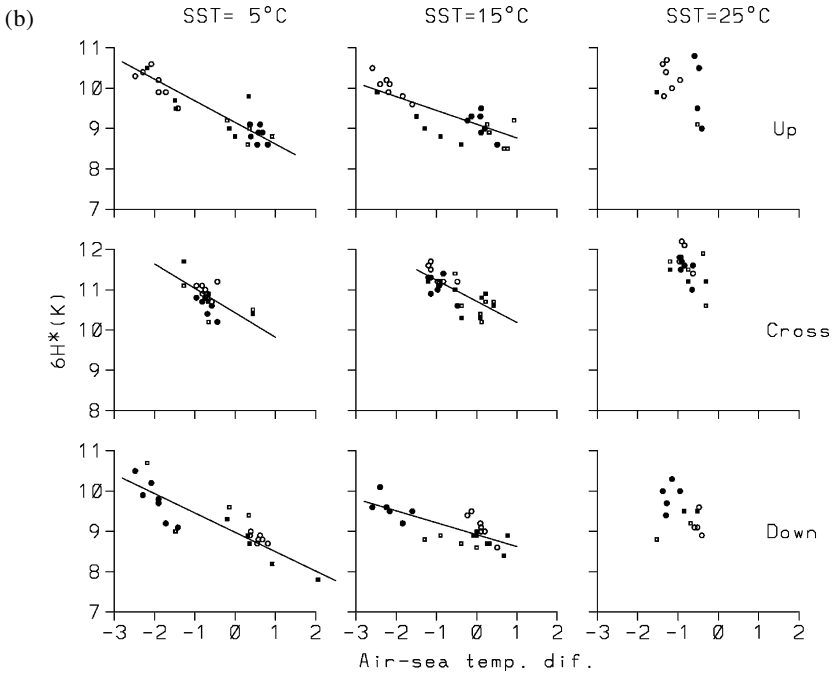

Fig. 1. (continued).

from shorelines. The ADEOS-II operating period of seven months was too short to combine the AMSR and buoy data. So we combined buoy data with the AMSR for the Earth Observing System (AMSR-E) data. The AMSR-E, which is almost identical to AMSR, is aboard the AQUA spacecraft launched by NASA in May 2002, and is operating at present. We use the AMSR-E data during 3.5 years from July 2002 to December 2005. In the latter combination we use the AMSR-E and buoy data, without the SeaWinds and others.

3. Data Analysis

We seek to obtain a relation between the ocean Tb and the air-sea temperature difference at two frequencies, 6 and 10 GHz. The AMSR Tbs at these frequencies contain much information about the Earth's surface and atmosphere, and we should remove two main effects from these AMSR Tbs: the atmospheric and SST effects. 6V(H)* defined by Eq. (1) combines the parameters that we investigate.

$$6V(H)^* = \text{AMSR\_6V(H)} - \text{atmos\_effect\_6V(H)} - \text{calm\_ocean\_6V(H)}, \quad (1)$$

where AMSR_6V(H) is the AMSR Tb at 6 GHz, atmos_effect_6V(H) is the atmospheric correction on 6 GHz, and calm_ocean_6V(H) is the ocean Tb at 6 GHz under calm conditions. The parameter atmos_effect_6V(H) is given by specifying the AMSR Tb of 23V, 36V, and SST. It removes the effects of water vapor, oxygen, and cloud liquid water in the atmosphere. It also excludes rainy areas by setting the upper limit of atmos_effect_6V(H). The parameter calm_ocean_6V(H) is defined as SST $\times (1 - r)$, where r is the Fresnel reflection coefficient with V-pol and H-pol. A detailed explanation of these two parameters was presented in our previous paper (Shibata, 2006). Units of 6V(H)* are Kelvin.

6V(H)* represents changes of the ocean Tb from the calm condition, induced by the ocean surface wind, or possibly by the air-sea temperature difference. Equation (1) corresponds to 6 GHz, and 10V(H)* corresponding to 10 GHz can be defined similarly.

In combining the AMSR and SeaWinds data, we took monthly averages of 6V(H)* to capture global-scale features of Tbs. In taking the monthly averages we divided global data according to five categories. The first one is SST, and we divided data into three SST: 5°C (2.5 to 7.5°C), 15°C (12.5 to 17.5°C), and 25°C (22.5 to 27.5°C). The second one is the satellite orbit, and we divided data into the ascending and descending orbits. On the ascending orbits the AMSR viewed northward. Among the AMSR viewing angles, data at azimuth angles between –20° (or 340°) and 20° were used, where 0° means north. On the descending orbits, the AMSR viewed southward. Data at azimuth angles between 160° and 200° were used, where 180° means south. The third category is the relative wind direction, which is defined as a relative angle between the AMSR viewing direction and SeaWinds wind

direction. The upwind direction is defined by angles between –20° and 20°, where 0° indicates an opposite direction. The crosswind direction is defined between 70° and 110° (also 250° and 290°), and the downwind one is between 160° and 200°. The fourth one is the hemisphere, and we divided data into the northern and southern hemispheres. The fifth one is the SeaWinds wind speed, and we divided data into nine wind speeds from 6 m/s to 14 m/s with 1 m/s interval. A wind speed of 14 m/s means a wind speed between 13.5 and 14.5 m/s. Finally, we took monthly averages for seven months from April to October 2003, according to the five categories described above.

We also averaged the air-sea temperature difference monthly for seven months using the GANAL air temperature and Reynolds SST. The averaging was done according to three categories: SST, hemisphere, and wind direction. The wind direction (northerly, southerly, and easterly/westerly winds) was determined using the GANAL wind direction. The northerly wind direction implies azimuth angles between –30° (or 330°) and 30°, where 0° means north; the southerly between 150° and 210°, where 180° means south; the easterly between 60 and 120 degrees; and the westerly between 240° and 300°.

In combing the AMSR-E and buoy data, the time difference between the AMSR-E and buoy measurements was limited to one hour or less. Definitions of the relative wind direction between the buoy wind direction and AMSR-E viewing direction were the same as the SeaWinds case. Nine-pixel data of the AMSR-E were averaged around the buoy location. To remove spatially non-uniform data, cases where the difference between the maximum and minimum values of 6H* exceeds 2K were omitted.

4. Results

First we look at results from a data combination of AMSR, SeaWinds, GANAL, and Reynolds SST in the global ocean. Then we look at results from a data combination of AMSR-E and buoys, which support the results for the global ocean. Finally, we apply our results to the AMSR SST algorithm.

4.1 Global analysis

We show comparisons between 6V(H*) and the air-sea temperature difference. Figure 1(a) compares 6V* and the air-sea temperature difference, in three relative wind directions and at three SSTs, which are all at the SeaWinds wind speed of 14 m/s. Figure 1(b) compares 6H* and the air-sea temperature difference. The most left panel corresponds to SST 5°C, the middle one to 15°C, and the right one to 25°C. The upper panel corresponds to the upwind direction, the middle one to the crosswind direction, and the bottom one to the downwind direction. As inferred in the introduction, we find that 6V(H)* vary with the air-sea temperature difference, i.e., 6V(H)* are negatively correlated with the air-sea temperature difference. From the results of Fig. 1, we assume that 6V(H)* is linearly related to the air-sea temperature, as defined by Eq. (2).

Table 1(a). Values of a and b for 6(10)V* (upper; a, lower; b).

		Up	Cross	Down
6V*	5℃	3.44	2.97	2.15
		0.38	0.51	0.45
	15℃	3.45	3.19	2.29
		0.24	0.44	0.28
10V*	5℃	3.84	3.31	2.48
		0.42	0.62	0.56
	15℃	3.99	3.61	2.72
		0.31	0.56	0.35

Table 1(b). Values of a and b for 6(10)H*.

		Up	Cross	Down
6H*	5℃	9.15	10.42	8.98
		0.54	0.61	0.48
	15℃	9.10	10.71	8.82
		0.34	0.53	0.30
10H*	5℃	11.48	13.13	11.58
		0.62	0.78	0.57
	15℃	11.01	13.27	11.28
		0.46	0.70	0.35

$$6V(H)^* = a - b \times \Delta T, \tag{2}$$

where, ΔT is the air-sea temperature difference. Coefficients a and b in Eq. (2) were determined independently at two SSTs of 5 and 15°C, and in three relative wind directions. In determining coefficients a and b, we used 6V* and 6H* simultaneously, under the constraining condition that the slope of 6H* to 6V* is preserved (see later in Fig. 4). Table 1(a) lists coefficients a and b for 6V*. Table 1(b) lists coefficients for 6H*. Regression lines at 25°C SST were not obtained since the air-sea temperature lies in a narrow range at 25°C SST.

We now look at the relations of 6V* and 6H* in Figs. 2, 3, and 4. The 6V*-6H* relations are important in retrieving accurate AMSR SST. Figure 2 shows the 6V*-6H* relations under several wind speeds from 6 to 14 m/s with 2 m/s intervals, and in three relative wind directions. The most left panel corresponds to 6 m/s, and the most right one to 14 m/s. The upper panel corresponds to the upwind direction, the middle one to the crosswind

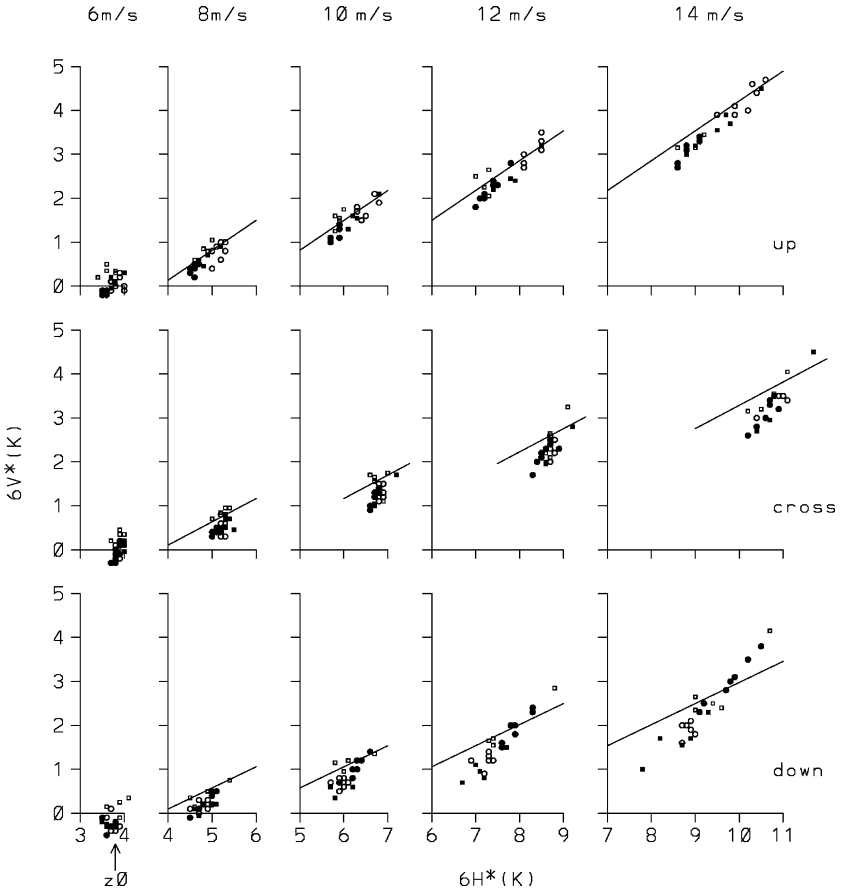

Fig. 2. Relations between 6V* and 6H* at several wind speeds and in three relative wind directions.

direction, and the bottom one to the downwind direction. All data in Fig. 2 are at SST of 5°C. Thin lines depicted in Fig. 2 are obtained from data in the global ocean for seven months: each line corresponds to the upwind direction with a slope of 0.68 in the upper panel, to the crosswind direction with a slope of 0.53 in the middle panel, and to the downwind direction with a slope of 0.48 in the bottom panel. We note three points in Fig. 2. The first one is that at lower wind speeds such as 6 m/s, data of 6V* and 6H* are gathered at one point, and they spread as the wind speed increases. At the wind speed of 6 m/s, 6H* reaches about 3.8 K (called z0), while 6V* remains at 0 K. The second point is that 6V* and 6H* are aligned almost on one line, for 6H* exceeding z0. This feature becomes clearer as the wind speed increases. The third point is that 6V* and 6H* in the downwind and crosswind directions are aligned with different slopes from the global ocean one, but those in the upwind direction are aligned with a similar slope to the global ocean one.

Figure 3 depicts an enlargement of the 6V*-6H* relation in Fig. 2 at the SeaWinds wind speed of 14 m/s in the downwind direction. Four symbols displayed in Fig. 3 represent ascending (A) or descending (D) orbits, and northern (N) or southern (S) hemispheres. A solid circle represents A/S, an open circle represents D/S, a solid square represents A/N, and an open square represents D/N. There are seven data points for A/S, but only five for the other cases. The data became less accurate for some months, since a strong wind of 14 m/s blew rarely. A thin line with a slope of 0.48 is plotted. We find that A/S and D/S data are separated (also A/N and D/N), and consider the reason as follows. In the downwind direction, the A/S data imply a southerly wind, and D/S data imply a northerly one, both in the southern hemisphere. The southerly wind is generally colder than the northerly one in the southern hemisphere. We see that the A/S data are located above the D/S data. In the northern hemisphere the situation is reversed, and the positions of A/N and D/N are reversed. This consideration governed the direct comparison of 6V(H)* and the air-sea temperature difference as shown in Fig. 1. In Figs. 1 and 2, data are displayed using the four symbols explained in Fig. 3. We see that the positions of four symbols are reversed between the downwind and upwind directions.

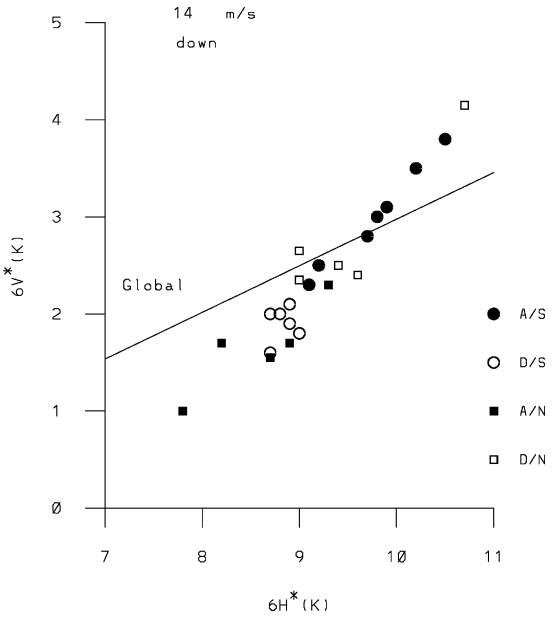

Fig. 3. Enlargement of Fig. 2, at SeaWinds wind speed of 14 m/s in the downwind direction.

Figure 4 depicts the 6V*-6H* relations at three SSTs, and in three relative wind directions, at the SeaWinds wind speed of 14 m/s. In the same relative wind direction, 6V* and 6H* seem to be aligned on one line even if SSTs are different. Regression lines are plotted in Fig. 4 for each relative wind direction, using all three SST data. The slope of the regression line is 0.70, 0.84, and 0.94, in the up-, cross-, and downwind directions, directly.

Finally, Fig. 5 depicts relations between 10V* and 10H*, corresponding to Fig. 2. Similar features are found to those described for 6V(H)*. Thin lines represent the slopes in the global ocean, with values of 0.58, 0.40, and 0.37, respectively, in the up-, cross-, and downwind directions. The ratio of Tb amplitude at 6 GHz to that at 10 GHz is estimated as 1.15. We also have similar results for the slopes corresponding to Fig. 4, with values at 10 GHz of 0.68, 0.80, and 0.99. 10V(H)* are also negatively correlated with the air-sea temperature difference, and Tables 1(a) and (b) includes coefficients *a* and *b* for 10V* and 10H*.

4.2 Buoy analysis

In the global analysis in Subsection 4.1, we saw the negative correlation between 6V(H)* and air-sea temperature difference for SST of 5 and 15°C, in which the sensitivity to the air-sea temperature difference at 5°C is

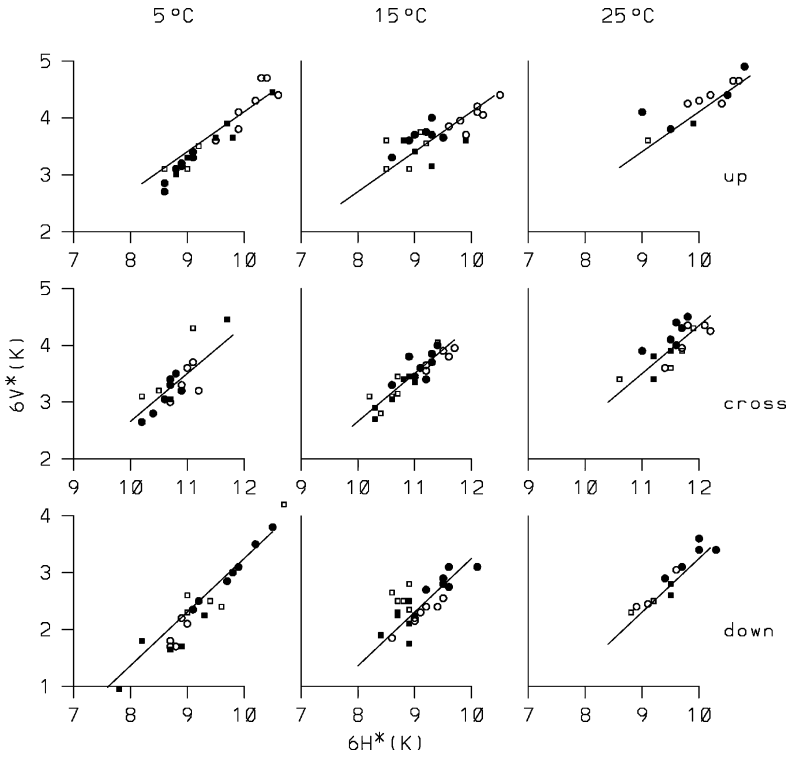

Fig. 4. Relations between 6V* and 6H* at three SSTs in three relative wind directions, obtained at SeaWinds wind speed of 14 m/s.

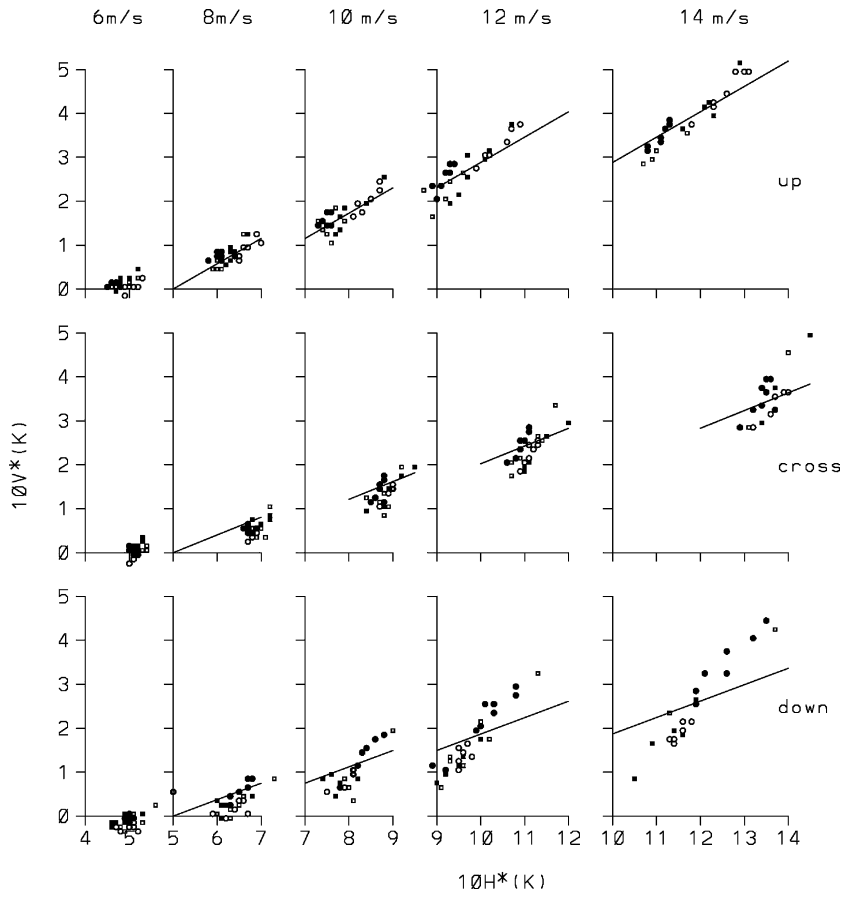

Fig. 5. Relations between 10V* and 10H* under the same geophysical conditions as Fig. 2.

greater than that at 15°C. Wind speed of SeaWinds used for this analysis represents the value at 10 m height above the sea surface. From our collocated data set of buoy and AMSR-E, only one buoy matched both the 10 m height anemometer and the lower SST, No. 46035 of NDBC, located in the center of the Bering Sea. In Fig. 6, the comparison between 6V* and air-sea temperature difference obtained from buoy 46035 is shown for the crosswind direction (Fig. 6(a)), and for the downwind direction (Fig. 6(b)), at the buoy wind speed of 14 m/s. SST of buoy 46035 ranged from 2.4 to 5.1°C. We see that 6V* is negatively correlated with the air-sea temperature difference, similarly to Fig. 1(a) of the global analysis. Regression lines are drawn in Figs. 6(a) and (b); coefficients *a* and *b* of the regression lines are 2.58 and 0.35 in the crosswind direction, and 2.09 and 0.43 in the downwind direction. These values almost coincide with those listed in Table 1(a) of the global analysis. For other buoys with different height anemometer, wind speeds were converted to those at a reference height of 10 m. In this conversion, the air-sea temperature difference was taken into account, following Liu and Tang (1996). To match SST of buoy 46035, SST for other buoys were limited at 10°C or less. Three buoys matched this SST condition: Nos. 46001, 44011, and 46005 of NDBC. SST for these buoys ranged from 3.6 to 9.8°C. The anemometers of those buoys were at 5 m height above the sea surface. Since the humidity data were absent for almost all collocated data, the humidity was set to a constant 70%. In Fig. 6(c), comparison between 6V* and air-sea temperature difference is shown for the crosswind direction, and we find a similar result to buoy 46035; coefficients a and b in this case are 3.33 and 0.37. In the downwind direction (Fig. 6(d)) we could not draw a regression line, since the air-sea temperature difference lay in a narrow range. For the upwind direction we had poor results for both buoy 46035 and the others, since the air-sea temperature difference also lay in a narrow range. For buoys with SST above 10°C, results were similar, and negative correlations between 6V* and air-sea temperature difference were found, although it was still difficult to determine accurate regression coefficients due to the small number of collocated data.

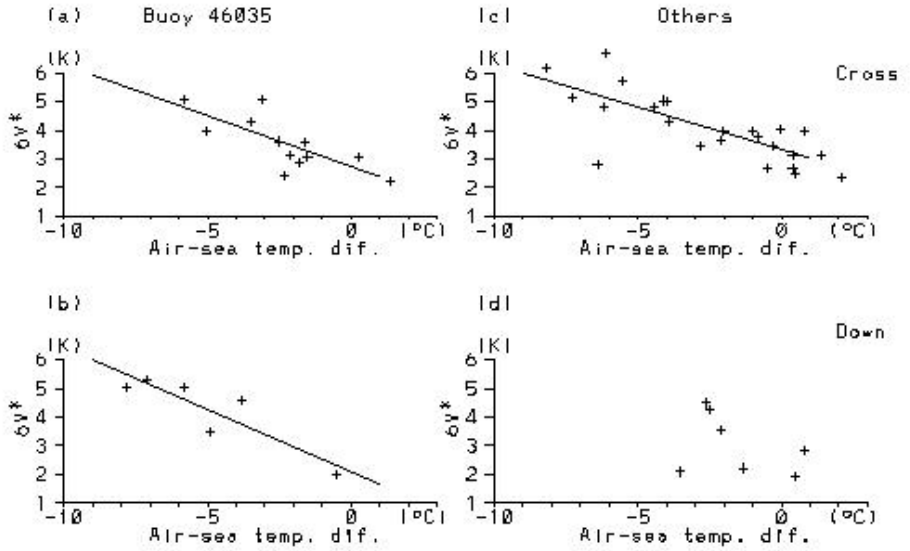

Fig. 6. Relation between 6V* and air-sea temperature difference, obtained at buoy wind speed of 14 m/s, in the downwind and crosswind directions, at SST less than 10°C. (a) and (b) are for buoy 46035 with the 10 m height anemometer, and (c) and (d) are for other buoys with the 5 m height anemometer.

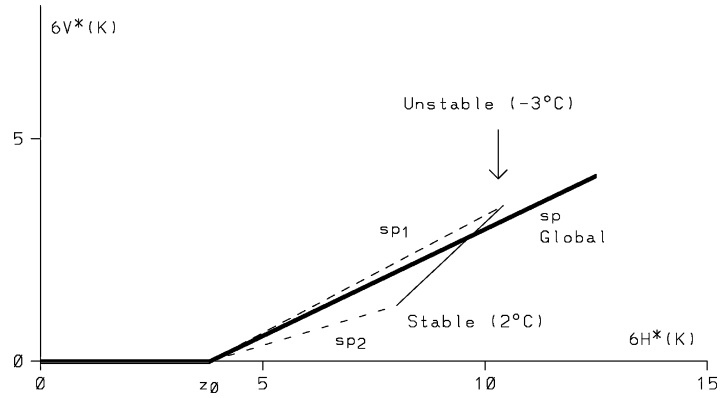

Fig. 7. Schematic method of wind correction in AMSR SST algorithm in case of the downwind direction.

4.3 Application of result to AMSR SST algorithm

We apply our results to the wind effect correction used in the AMSR SST algorithm. In this correction, the slope of 6H* to 6V*, sp, is important to retrieve the accurate SST. We express sp by Eq. (3).

$$sp = 6V^*/(6H^* - z0). \quad (3)$$

Figure 7 depicts a schematic method for the wind correction. The 6V*-6H* relation in the global ocean in the downwind direction is shown as a bold line. The AMSR SST is retrieved from AMSR_6V, because the sensitivity of the vertical polarization to SST is greater than twice that of the horizontal polarization. 6H* is used to remove the wind effect on AMSR_6V. The 6V*-6H* relation in Fig. 7 indicates that 6V* remains at 0K until 6H* reaches z0, and it increases with the slope of sp above z0.

In Fig. 7, additional (dotted) lines are depicted for two cases of negative and positive air-sea temperature differences. The slope of sp_1 represents the negative (unstable) air-sea temperature difference, and its slope is calculated using Eqs. (2) and (3) with ΔT of –3°C. The slope of sp_2 represents the positive (stable) case, and it is calculated with ΔT of 2°C. A thin line represents positions of 6V* and 6H* with ΔT varying from –3°C to 2°C. Figure 7 implies that sp varies with the air-sea temperature difference ΔT. This result supports two findings of our previous paper: one is that sp varies seasonally and

latitudinally, and the other is that different values of sp should be applied in areas with extreme positive or negative air-sea temperature differences. As seen in Fig. 2, 6V* and 6H* are aligned on a different slope from the global ocean one, in the downwind and crosswind directions. Those in the upwind direction, however, are aligned on a similar slope to the global ocean one. Therefore, the effect of the air-sea temperature difference is dominant in the former two cases, but not in the latter case.

5. Conclusions and Discussion

The effect of the air-sea temperature difference on the ocean Tb was investigated by two methods. The first is to combine the data of the AMSR, SeaWinds, both aboard ADEOS-II, GANAL, and Reynolds SST. The second one is to combine the data of the AMSR-E aboard the AQUA and ocean buoys. Parameters of 6V(H)* were defined for 6 GHz, which were derived from the AMSR Tbs, corrected for the atmospheric and SST effects. Parameters of 10V(H)* were also defined for 10 GHz.

In the first method, 6V(H)* were averaged monthly, according to five categories: SST, satellite orbits, relative wind directions, hemispheres, and SeaWinds wind speed. The relative wind direction was defined as the angle made by the AMSR viewing angle and SeaWinds wind direction. The air-sea temperature difference was also averaged monthly according to similar categories, using the GANAL air temperature and the Reynolds SST, in which the GANAL wind direction was used to classify the wind direction. Direct comparisons of 6V(H)* with the air-sea temperature difference revealed that they are negatively correlated. The ratios of the air-sea temperature difference to 6V(H)* varied with the SST, and with the relative wind direction. Ratios of the air-sea temperature to 6V*, averaged among the three relative wind directions, were –0.45K/°C at SST 5°C and –0.32K/°C at SST 15°C, which were obtained at the SeaWinds wind speed of 14 m/s. Ratios for 6H* were –0.54K/°C at SST 5°C and –0.39K/°C at SST 15°C. In the plane of 6V* and 6H*, 6V* and 6H* were aligned on one line, and their slopes were independent of the three SSTs, but their slopes are different among the three relative directions. Features at 10 GHz were similar to those at 6 GHz. Ratios for 10V* were –0.53K/°C at SST 5°C and –0.41K/°C at SST 15°C, and those for 10H* were –0.66K/°C and –0.50K/°C, all obtained at the SeaWinds wind speed of 14 m/s.

In results obtained by the second method to combine the AMSR-E and buoy data, limited cases are shown. Comparison between 6V* and buoy with the 10 m height anemometer showed a similar result to the global analysis by the first method. Comparison between 6V* and other buoys with the 5 m height anemometer also showed similar a result, when wind speeds were converted to the 10 m height ones, taking account of the air-sea temperature difference.

The effect of the air-sea temperature difference on the wind correction in the AMSR SST algorithm was investigated. In the downwind and crosswind directions, 6V(H)* are aligned on different slopes from the global ocean one. In these cases, sp varies with the air-sea temperature difference, and this affects the accuracy of the AMSR SST. In the upwind direction, 6V(H)* are aligned on a similar slope to the global ocean one. In this case, sp does not vary significantly with the air-sea temperature difference, and it does not affect the AMSR SST.

As one possible mechanism to induce correlation between the ocean Tb and the air-sea temperature difference, we would like to point out the presence of the ocean foam. As mentioned in the introduction, Droppleman (1970) reported that the ocean Tb rises significantly when ocean foam is present, because the emissivity of the ocean foam is much higher than that of the ocean surface, i.e., foam raises the ocean Tb by a few Kelvin, even though the surface is covered with a few percent of foam. In further support of suggestion, the paper by Monaham and O'muircheartaigh (1986) is helpful. They reported that the whitecap coverage on the ocean surface varies with wind speed, with SST, and with air-sea temperature difference (ΔT). Following their results, the whitecap coverage is proportional to $\exp(-0.0861 \times \Delta T)$: the whitecap coverage decreases by 35%, in the case that ΔT increases by 5°C from –3°C to 2°C. In our case, foam affects the ocean Tbs, but we might compare our results with theirs, since foam and whitecap are closely related to each other. In Fig. 1, the ocean Tb decreases as ΔT increases, which qualitatively coincides with their results. We have expressed Tb decrease as a linear function rather than an exponential one. A relative Tb decrease of 6V*, averaged among the three wind directions, is 55% in the case of ΔT increasing by 5°C from –3°C to 2°C (see Fig. 1(a)). The difference between the two results (35% versus 55%) is not negligible, but might be acceptable, considering the preliminary nature of the comparison.

We would like to discuss why the AMSR Tbs are sensitive to the air-sea temperature difference. In our data analysis, the AMSR Tbs were classified according to the wind speed measured by the SeaWinds or ocean buoys. The SeaWinds wind speed is derived from a returned echo from the ocean surface, and it is related to a 10-meter height wind speed. The returned echo is closely related to capillary waves or short gravity waves with wavelengths of several centimeters on the ocean surface. We speculate that the intensity of these waves is less sensitive to the air-sea temperature difference, compared to the sensitivity of the ocean foam. On the other hand, the ocean foam affects the ocean Tb, and the ocean foam is strongly correlated with the air-sea temperature difference, which may be why the AMSR Tb is sensitive to the

air-sea temperature difference.

We found that the response of 6V* to the air-sea temperature, derived from the buoy comparison, is almost similar to that from the global analysis using the SeaWinds data. This result supports the idea that the GANAL air temperature is at a level that is usable for our data analysis. Furthermore, this result suggests that the SeaWinds wind speed is equal to a 10-meter height wind speed, almost independent of the air-sea temperature difference. The buoy comparison was made for a limited number of cases, so we should investigate further cases after accumulating more collocated data between the AMSR-E and buoys.

Acknowledgements

This work was supported by the ADEOS-II project with JAXA EORC. We are grateful to the Jet Propulsion Laboratory for providing us with the SeaWinds data.

References

Droppleman, J. D. (1970): Apparent microwave emissivity of sea foam. *J. Geophys. Res.*, **75**(3), 697–698.

Ebuchi, N. (2006): Evaluation of marine surface winds observed by SeaWinds and AMSR on ADEOS-II. *J. Oceanogr.*, **62**, 293–302.

Hollinger, J. P. (1971): Passive microwave measurements of sea surface roughness. *IEEE Trans. Geosci., Electron.*, **9**(3), 165–169.

Kawanishi, T. *et al.* (2003): The Advanced Microwave Scanning Radiometer for the Earth Observing System (AMSR-E), NASDA's contribution to the EOS for global energy and water cycle studies. *IEEE Trans. Geosci. Remote Sensing*, **41**, 184–194.

Liu, W. T. (2002): Progress in scatterometer application. *J. Oceanogr.*, **58**, 121–136.

Liu, W. T. and W. Tang (1996): Equivalent neutral wind. JPL Pub. 96-17, Jet Propulsion Laboratory, Pasadena, 16 pp.

Meissner, T. and F. Wentz (2002): An updated analysis of the ocean surface wind direction signal in passive microwave brightness temperatures. *IEEE Trans. Geosci. Remote Sensing*, **40**, 1230–1240.

Monaham, E. C. and I G. O'muircheartaigh (1986): Whitecaps and passive remote sensing of the ocean surface. *Int. Remote Sensing*, **7**(5), 627–642.

Reynolds, R. W. and T. M. Smith (1994): Improved global sea surface temperature analyses. *J. Climate*, **7**, 929–948.

Shibata, A. (2006): Features of ocean microwave emission changed by wind at 6 GHz. *J. Oceanogr.*, **62**(3), 321–330.

Swift, C. T. (1980): Passive microwave remote sensing of the ocean—a review. *Boundary-Layer Meteorology*, **18**, 25–54.

Wentz, F. J. (1983): A model function for ocean microwave brightness temperature. *J. Geophys. Res.*, **88**(C3), 1892–1908.